

# A Primary Noise Thermometer for Ultracold Bose Gases

R Gati, J Esteve, B Hemmerling, T B Ottenstein, J Appmeier,  
A Weller, M K Oberthaler

Kirchhoff-Institut für Physik, Universität Heidelberg, Im Neuenheimer Feld 227,  
69120 Heidelberg, Germany

E-mail: noisethermometry@matterwave.de

**Abstract.** We discuss in detail the experimental investigation of thermally induced fluctuations of the relative phase between two weakly coupled Bose-Einstein condensates. In analogy to superconducting Josephson junctions, the weak coupling originates from a tunneling process through a potential barrier which is obtained by trapping the condensates in an optical double-well potential. The observed fluctuations of the relative phase are in quantitative agreement with a many body two mode model at finite temperature. The agreement demonstrates the possibility of using the phase fluctuation measurements in a bosonic Josephson junction as a primary thermometer. This new method allows for measuring temperatures far below the critical temperature where standard methods based on time of flight measurements fail. We employ this new thermometer to probe the heat capacity of a degenerate Bose gas as a function of temperature.

PACS numbers: 03.75.-b, 05.40.-a, 74.40.+k, 74.50.+r

Submitted to: *NJP*

## 1. Introduction

Among other methods [1, 2], a stable double-well potential for Bose-Einstein condensates can be realized by superimposing a three-dimensional harmonic trapping potential and a one-dimensional optical lattice with large periodicity [3]. If the height of the potential barrier in the center of the trap becomes comparable to the chemical potential, the Bose-Einstein condensate (BEC) is split into two parts. If the barrier height is not too high, the two split condensates are still weakly coupled via tunneling through the barrier in analogy to superconducting Josephson junctions [4, 5] and superfluid Helium weak links [6].

At equilibrium, the relative phase between the two coupled condensates fluctuates because of quantum fluctuations [7, 8, 9] and thermally induced fluctuations [10]. The experiments discussed in this paper are performed in the so-called 'classical Josephson regime' where quantum mechanical fluctuations are negligible and thermally induced fluctuations can be treated classically. As shown in [10], the phase fluctuations in this regime depend only on a single parameter given by the ratio of the thermal energy and the tunneling coupling strength between the two wells.

The dependence of the phase fluctuations on temperature allows for the application of the fluctuation measurements for thermometry [11]. Hereby the coherence factor, *i.e.* the variance of the phase fluctuations, is measured experimentally and compared to the theoretical prediction. Standard methods to estimate temperature in Bose-Einstein condensed atomic samples usually rely on time of flight measurements. The temperature is deduced after ballistic expansion either from the expansion velocity of the thermal cloud or from the ratio of the condensed to the non-condensed populations. This method starts to fail for temperatures far below the critical temperature where the number of particles in the thermal cloud becomes small compared to the number of particles in the BEC. However, even in this regime, the phase fluctuation method can be applied as the coupling strength can be tuned via the barrier height in order to make the bosonic Josephson junction (BJJ) sensitive to thermally induced effects.

Experimentally the relative phase between the Bose-Einstein condensates can be accessed by time of flight during which the two condensates expand and interfere [12]. The resulting density profile is analogous to the intensity profile observed with coherent light in double-slit interference experiments and the relative phase can be deduced from the position of the interference peaks with respect to their envelope. Interference patterns are observable for any temperature as far as the Bose-Einstein condensate fraction is large enough for detection. Hereby the visibility of the patterns increases with decreasing temperature making the investigation of the thermally induced fluctuations accessible for a wide range of temperatures.

Thermally induced phase fluctuations have been observed so far in elongated Bose-Einstein condensates [13, 14]. In these quasi 1-D BEC the coherence of the whole cloud is diminished by the thermally populated low lying excitations. In time of flight these excitations are revealed as density fringes on the BEC envelope. For low

temperatures the contrast of the fringes decreases and vanishes when the typical length of the phase fluctuations becomes larger than the longitudinal extent of the condensate. The situation in the presented double-well potential is different. Here only the coherence between the two wells is affected by thermal processes and not the coherence within each well. The fluctuations decrease and vanish for very low temperatures but increases for raising the barrier height.

## 2. Phase fluctuations within the two mode approximation

In order to use the phase fluctuation measurement as a tool for thermometry, a precise theoretical model is needed to convert the measured fluctuations into a temperature. In this section, we present in detail the two mode model that we use for this purpose. In this model, the condensate particles can occupy only two single particle states while being in thermal equilibrium with a bath composed of the non condensed atoms. We will first shortly introduce the two mode model which has attracted tremendous interest in the literature (see references 2 to 20 in [15]). We will then show that, because of its relative simplicity, this model allows exact numerical calculations of the phase fluctuations (or any other quantity) at finite temperature. The drastic reduction of the Hilbert space dimension due to the two mode approximation makes the two mode model one of the few exactly numerically solvable many body systems (see for example [16, 17, 18]). We will compare our numerical results with analytical results that can be obtained in the low temperature and the high temperature limit.

### 2.1. The two mode approximation

Starting from the general many body problem of a gas of interacting bosons, the two mode approximation consists of restricting the available single particle states to two states  $|\phi_1\rangle$  and  $|\phi_2\rangle$ . Fixing the total atom number in the sample to a given value  $N$ , a basis of the system can then be obtained by considering the following set of Fock states

$$|n\rangle = |N - n : \phi_1, n : \phi_2\rangle \quad \text{where } n = 0, 1, \dots, N. \quad (1)$$

The dimension of the Hilbert space is then reduced to  $N + 1$ . This drastic reduction of the dimension allows exact numerical quantum calculations for the atom number range accessed in our experiments ( $N < 10^4$ ).

The double-well trap used in our experiment naturally provides a geometry where the two mode approximation can be applied. Indeed, a Bogoliubov calculation of the excitation spectrum or a calculation of the Gross-Pitaevskii eigenenergies shows that the first excitation lies close to the ground state while the second excitation is well above. As in the non-interacting case, such a situation occurs only if the barrier separating the two condensates is sufficiently high (higher than the chemical potential in each well). Supposing this condition to be fulfilled, we choose for the two single particle states  $|\phi_1\rangle$  and  $|\phi_2\rangle$ , the first two eigenstates of the Gross-Pitaevskii equation  $|\phi_s\rangle$  and  $|\phi_a\rangle$ :  $|\phi_s\rangle$

being the symmetric ground state and  $|\phi_a\rangle$  the antisymmetric first excited state<sup>‡</sup>. The corresponding eigenvalues are given by

$$\mu_{s,a} = \int \phi_{s,a}^* \left( -\frac{\hbar^2}{2m} \nabla^2 + V + gN|\phi_{s,a}|^2 \right) \phi_{s,a} d\mathbf{r}. \quad (2)$$

where  $g$  is the effective interaction strength in 3-D.

Introducing the creation operators  $\hat{c}_s^\dagger$  and  $\hat{c}_a^\dagger$  associated with the two wavefunctions  $\phi_s$  and  $\phi_a$ , the field operator writes in the two mode approximation

$$\hat{\Psi} = \hat{c}_s \phi_s + \hat{c}_a \phi_a. \quad (3)$$

Starting from the many body Hamiltonian

$$\hat{H} = \int \left( \hat{\Psi}^\dagger \left( -\frac{\hbar^2}{2m} \nabla^2 + V \right) \hat{\Psi} + \frac{g}{2} \hat{\Psi}^\dagger \hat{\Psi}^\dagger \hat{\Psi} \hat{\Psi} \right) d\mathbf{r}, \quad (4)$$

and ignoring constant terms (terms proportional to the total atom number), we obtain the following two mode Hamiltonian [15, 19]

$$\hat{H}_{2M} = -\frac{E_J}{N} (\hat{c}_s^\dagger \hat{c}_s - \hat{c}_a^\dagger \hat{c}_a) + \frac{E_C}{8} (\hat{c}_s^\dagger \hat{c}_a + \hat{c}_a^\dagger \hat{c}_s)^2 + \frac{\delta E_C}{4} (\hat{c}_s^\dagger \hat{c}_s - \hat{c}_a^\dagger \hat{c}_a)^2 \quad (5)$$

$$= -\frac{E_J}{N} (\hat{c}_l^\dagger \hat{c}_r + \hat{c}_r^\dagger \hat{c}_l) + \frac{E_C}{8} (\hat{c}_r^\dagger \hat{c}_r - \hat{c}_l^\dagger \hat{c}_l)^2 + \frac{\delta E_C}{4} (\hat{c}_l^\dagger \hat{c}_r + \hat{c}_r^\dagger \hat{c}_l)^2. \quad (6)$$

The last equality expresses the Hamiltonian in terms of creation and annihilation operators in the left/right basis which we define as  $\hat{c}_l^\dagger = (\hat{c}_s^\dagger + \hat{c}_a^\dagger)/\sqrt{2}$  and  $\hat{c}_r^\dagger = (\hat{c}_s^\dagger - \hat{c}_a^\dagger)/\sqrt{2}$ . The Josephson energy  $E_J$ , the charging energy  $E_C$  and the correction term  $\delta E_C$  are defined as follow

$$\kappa_{i,j} = \frac{g}{2} \int |\phi_i|^2 |\phi_j|^2 d\mathbf{r} \quad (\text{with } i, j = s, a) \quad (7)$$

$$E_C = 8\kappa_{s,a} \quad (8)$$

$$E_J = \frac{N}{2} (\mu_a - \mu_s) - \frac{N(N+1)}{2} (\kappa_{a,a} - \kappa_{s,s}) \quad (9)$$

$$\delta E_C = \frac{\kappa_{s,s} + \kappa_{a,a} - 2\kappa_{s,a}}{4}. \quad (10)$$

The first term of the two mode Hamiltonian which is proportional to  $E_J$  describes the tunneling between the two wells. It is diagonal in the symmetric/antisymmetric basis. The second term proportional to  $E_C$  describes the on-site interaction in each well and is diagonal in the left/right basis. The last term is a correction term that, as we will see, can usually be neglected.

In the high barrier limit, the different interaction coefficients  $\kappa_{i,j}$  can be considered to be equal and the correction term  $\delta E_C$  vanishes. In our experimental parameter range, we find this term to be less than  $10^{-5} \cdot E_J/N$  and less than  $10^{-3} \cdot E_C/8$ . The correction term is included in our numerical calculations, however its effect is so small that we will neglect it in the following discussion. To obtain the values of these three coefficients, we numerically solve the 3-D Gross Pitaevskii equation in our potential using a standard split-step iteration algorithm and propagation in imaginary time. The precision of the

<sup>‡</sup> We assume the wavefunctions  $\phi_s$  and  $\phi_a$  to be normalized to one.

calculated values directly relies on the numerical precision of the employed method. In particular, the Josephson energy requires special care, because it critically depends on the difference of two energies  $\mu_s$  and  $\mu_a$  which are almost degenerate.

*2.1.1. Eigenenergy spectrum* As mentioned above, the limited size of the Hilbert space allows exact numerical diagonalization of the two mode Hamiltonian. Our experimental parameter range is such that we always lie in the Josephson regime where the two conditions  $E_C \ll E_J$  and  $E_C \gg E_J/N^2$  are fulfilled. In this regime, a typical energy spectrum of the many body system looks like the one shown in Fig. 1. (a). At low energy ( $E < 2E_J$ ), the spectrum is almost linear and the level spacing is approximately given by the plasma frequency (see Fig. 1 (b))

$$\omega_p = \frac{1}{\hbar} \sqrt{E_J \left( E_C + \frac{4E_J}{N^2} \right)}. \quad (11)$$

The corresponding eigenstates are delocalized over the two wells (see Fig. 1 (c)). In a classical picture, where the two mode Hamiltonian corresponds to the Hamiltonian of a pendulum, these states correspond to an oscillatory motion of the pendulum around its equilibrium (see Fig. 1 (d)). At higher energy ( $E > 2E_J$ ), the eigenenergies are grouped two by two. Each doublet of almost degenerate eigenstates consists of a state localized in the left well and one localized in the right well (see Fig. 1 (c)). In the classical picture, these states correspond to a twirling motion of the pendulum and the degeneracy corresponds to the two possible directions of rotation. The energy of these states is dominated by the charging energy term and thus increases quadratically with the eigenstate label as expected for a free particle motion.

## 2.2. Calculation of the coherence factor

As we will show now, our measurement of the phase fluctuations is a direct measurement of the coherence of the system. The coherence of a many body system can be quantitatively measured by considering the first order spatial coherence function  $g^{(1)}(\mathbf{r}, \mathbf{r}')$ . In the two mode approximation, it is easy to see from (Eq. 3) that the first order spatial coherence function does not depend on the difference  $(\mathbf{r} - \mathbf{r}')$  and is constant [19]. We can then unambiguously define the coherence of the system  $\alpha$  as the uniform value of the spatial coherence function.

$$\begin{aligned} \alpha = g^{(1)}(\mathbf{r}, \mathbf{r}') &= \frac{\langle \hat{\Psi}^\dagger(\mathbf{r}') \hat{\Psi}(\mathbf{r}) \rangle}{\sqrt{\langle \hat{\Psi}^\dagger(\mathbf{r}') \hat{\Psi}(\mathbf{r}') \rangle \langle \hat{\Psi}^\dagger(\mathbf{r}) \hat{\Psi}(\mathbf{r}) \rangle}} \\ &= \frac{\langle \hat{c}_l^\dagger \hat{c}_r + \hat{c}_r^\dagger \hat{c}_l \rangle}{N} = \frac{\langle \hat{c}_s^\dagger \hat{c}_s - \hat{c}_a^\dagger \hat{c}_a \rangle}{N}. \end{aligned} \quad (12)$$

In the two mode approximation, the coherence of the system is simply given by the relative population difference between the symmetric and the antisymmetric state.

The equivalence between the coherence factor defined above and the mean fringe visibility can be established in the following way. In the two mode approximation,

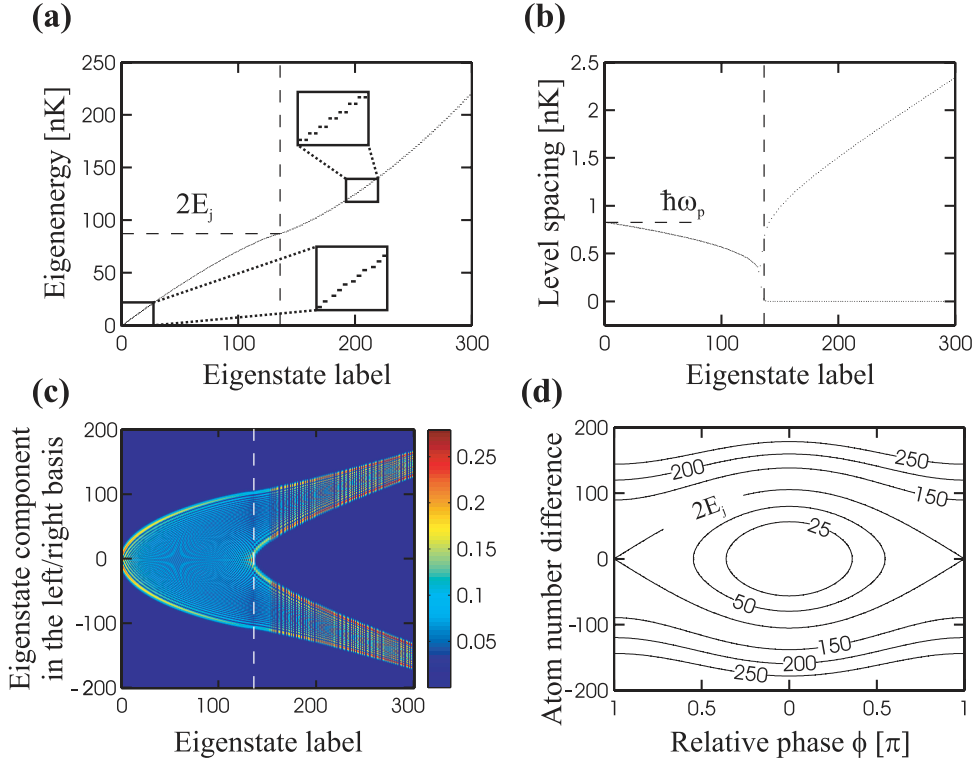


**Figure 1.** Lower energy eigenvalues and eigenstates of the two mode Hamiltonian in the Josephson regime ( $E_C = 0.016$  nK,  $E_J = 43$  nK and 3000 atoms): (a) eigenenergies, (b) eigenenergy differences, (c) eigenstates components in the left/right Fock state basis  $|N/2 - n : \text{left}, N/2 + n : \text{right}\rangle$ , (d) Phase portrait of the classical pendulum associated with the two mode model for different total energies. At low energy ( $E < 2E_J$ ), the linear part of the spectrum corresponds to an oscillatory motion in the pendulum picture and the associated eigenstates are delocalized in the left/right basis. At higher energy, each level is two times degenerate, which corresponds to the two possible rotation directions of the pendulum twirling motion. The associated eigenstates are well localized in one well.

the Fourier component of the field operator is  $\hat{\Psi}(\mathbf{k}) = \hat{c}_s \phi_s(\mathbf{k}) + \hat{c}_a \phi_a(\mathbf{k})$ . The Fourier transform of the symmetric and the antisymmetric state correspond to fringe patterns with respectively a zero (bright central fringe) and a  $\pi$  phase (dark central fringe) modulated by an envelope  $f(\mathbf{k})$ . The mean atom velocity distribution can thus be written as

$$\begin{aligned}
 n(\mathbf{k}) &= \langle \hat{\Psi}^\dagger(\mathbf{k}) \hat{\Psi}(\mathbf{k}) \rangle \\
 &= n_s \phi_s(\mathbf{k}) + n_a \phi_a(\mathbf{k}) \\
 &= \left[ 1 + \frac{n_s - n_a}{N} \cos(k_x d) \right] f(\mathbf{k}) = [1 + \alpha \cos(k_x d)] f(\mathbf{k}), \quad (13)
 \end{aligned}$$

where  $\alpha$  is the visibility of the interference patterns. Assuming that the interactions do not significantly modify the velocity distribution of the atoms after a time of flight, Eq. 13 shows that the mean visibility factor is equal to the relative population difference between the symmetric and antisymmetric states and thus to the coherence factor  $\alpha$

(Eq. 12). Note that this approach does not allow for making any prediction on the fringe contrast observed after a single experiment, which is always expected to be high.

### 2.3. Low temperature limit

We define the low temperature regime as the range corresponding to temperatures on the order of the plasma frequency up to the Josephson energy. In this regime, both quantum and thermal fluctuations play a role, but their overall contribution is small enough so that the coherence factor is close to 1. Following a Bogoliubov approach, we can calculate analytically the expression of the coherence factor. As shown in [20], starting from the two mode Hamiltonian, the Bogoliubov transformation is straightforward since only one quasiparticle mode can exist. The transformed Bogoliubov Hamiltonian writes

$$\hat{H}_{\text{Bg}} = E_{\text{Bg}}(N) + \hbar\omega_p(\hat{g}^\dagger\hat{g} + 1/2). \quad (14)$$

$E_{\text{Bg}}(N)$  is a constant energy term. The excitation creation operator is  $\hat{g}^\dagger = u\hat{c}_a^\dagger + v\hat{c}_a$  where  $u = \cosh \chi$ ,  $v = \sinh \chi$  and  $\tanh 2\chi = E_C/(E_C + 8E_J/N^2)$  [20]. The obtained excitation spectrum corresponds to the linear part of the exact spectrum plotted in Fig. 1 (a).

To determine the coherence factor, we calculate the number of atoms in the antisymmetric state by

$$\begin{aligned} n_a &= \langle \hat{c}_a^\dagger \hat{c}_a \rangle \\ &= \langle \hat{g}^\dagger \hat{g} \rangle (u^2 + v^2) + v^2. \end{aligned} \quad (15)$$

We find the usual formula for the condensate depletion: the first term corresponds to thermal fluctuations and the second term to quantum depletion. The coherence factor is then

$$\langle \alpha \rangle = 1 - 2\frac{n_a}{N} \simeq 1 - \frac{1}{2}\sqrt{\frac{E_C}{E_J}} \left( \frac{1}{\exp(\beta\hbar\omega_p) - 1} + \frac{1}{2} \right). \quad (16)$$

with  $\beta = (k_B T)^{-1}$ . In the last equality, we have used the assumption that we are in the Josephson regime ( $E_J/N^2 \ll E_C$ ). The decoherence due to quantum fluctuations is proportional to  $\sqrt{E_C/E_J}$  and is always small in the Josephson regime. In Fig. 2, we compare this analytical result with an exact numerical calculation of  $\alpha$  for different temperatures. We observe that the Bogoliubov result is only verified when the condensate depletion is sufficiently small which corresponds to temperatures below the Josephson energy.

### 2.4. High temperature limit

For temperatures much higher than the mean level spacing, which is approximately given at low energy by the plasma energy, a semi-classical calculation of the thermal average fringe visibility is valid. The two mode Hamiltonian corresponds to the following classical Hamiltonian [21]

$$H_{\text{Cl}} = E_C \frac{n^2}{2} - E_J \sqrt{1 - \frac{4n^2}{N^2}} \cos \phi, \quad (17)$$

where  $n$  is half the atom number difference between the two wells and  $\phi$  is the relative phase between the two wells.

In this picture, the coherence factor corresponds to the mean value of  $\cos \phi$  which writes

$$\langle \cos \phi \rangle = \frac{1}{Z} \int \cos \phi \exp(-\beta H_{C1}) \quad \text{where} \quad Z = \int \exp(-\beta H_{C1}). \quad (18)$$

In the Josephson regime, the relatively strong interaction term prevents any contribution of large values of  $n$  in the previous integral. The coherence factor can then be approximated by ([10])

$$\alpha = \langle \cos \phi \rangle = \frac{\int \cos \phi \exp(-\beta E_J \cos \phi)}{\int \exp(-\beta E_J \cos \phi)} = \frac{I_1(\beta E_J)}{I_0(\beta E_J)}, \quad (19)$$

where  $I_i(j)$  are the modified Bessel functions of the first kind. Fig. 2 shows the comparison of this analytical expression with the exact numerical calculation for different temperatures and two different Josephson energies. At high temperature, the agreement is always very good. At low temperature and if the Josephson energy is smaller than approximately  $10E_C$ , a small discrepancy can appear because of quantum fluctuations (see right graph in Fig. 2). To use the coherence factor measurement for thermometry, we always place ourselves in the situation shown in the left graph of Fig. 2 where the agreement between the exact calculation and the semi-classical formula (Fig. 19) is better than 1%. In this case, the coherence factor only depends on the dimensionless parameter  $\beta E_J$ , the conversion between the two quantities being precisely given by Eq. 19. Since the phase fluctuations depend strongly on the temperature in the range of  $0.1E_J$  and  $10E_J$  (see grey shaded area in Fig. 2), this regime is ideally suited for deducing the temperature from phase fluctuation measurements. This dynamic range can furthermore be tuned by adjusting the coupling strength  $E_J$ . Once the parameter  $\beta E_J$  is known from the coherence measurement, the conversion to a temperature relies on a precise calculation of  $E_J$ . The main uncertainty in this calculation comes from the atom number uncertainty.

### 3. Experimental protocol

In this section, we give an overview of our experimental thermometry procedure. Our experimental setup has already been described in detail in [22]. The experiment is performed as follows. We first generate a single Bose-Einstein condensate by loading a precooled  $^{87}\text{Rb}$  sample in a 3-D optical dipole trap as indicated in Fig. 3 (a). The harmonic trapping frequencies are  $\omega_x = 2\pi \cdot 90(2)$  Hz and  $\omega_{y,z} = 2\pi \cdot 100(2)$  Hz. Evaporative cooling is performed until the number of particles in the trap is lowered usually to about 2000 to 4000 and the lowest accessible temperature  $T = 15(4)$  nK is reached. Holding the atoms in the trap for a given time allows for increasing the temperature of the sample in a controlled way. The heating rate in the optical trap is about 2 nK/s for a classical gas (see Sec. 6). Once the final temperature is reached, the harmonic potential is transformed into the double-well potential by slowly ramping up

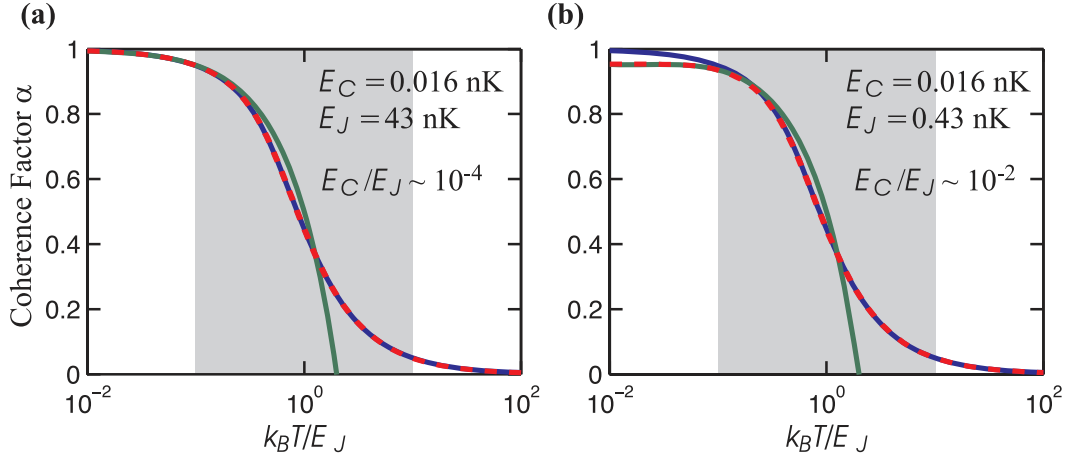


**Figure 2.** Coherence factor  $\alpha$  as a function of the ratio  $k_B T/E_J$  for 3000 atoms. The dashed red curve shows the result of the exact numerical calculation. The green curve is the Bogoliubov calculation (16) which is valid only at low temperature and correctly accounts for quantum fluctuations (right graph). The blue curve is the result of the semi-classical calculation (19) which is valid at high temperature and also at low temperature if quantum fluctuations are negligible (left graph). The grey shaded area corresponds to the region where the measurement of the coherence factor can be used for thermometry.

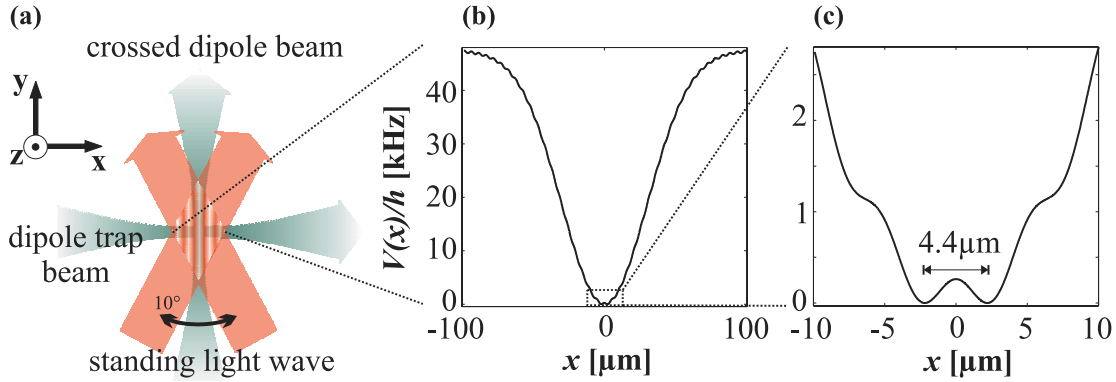


**Figure 3.** Experimental setup and realization of the double-well potential by the superposition of a harmonic trap and an optical lattice with large periodicity. (a) is a sketch of the laser beams generating the optical potentials. Two orthogonal dipole trap beams at 1064 nm (grey) create a 3-D harmonic confinement and two laser beams at 830 nm crossing under an angle of  $10^\circ$  generate the optical lattice (red) with a periodicity of  $\lambda = 4.8 \mu\text{m}$ . (b) shows the effective potential resulting from the superposition of the dipole trap and the optical lattice on the scale of the Gaussian dipole trap beam. (c) is the potential in the center of the trap revealing the effective double-well trap with a separation of the two wells of  $4.4 \mu\text{m}$ .

a standing light wave of the form  $V = V_0/2 \cdot (1 + \cos(2\pi \cdot x/\lambda))$  with  $\lambda = 4.8(2) \mu\text{m}$ . The resulting potential is shown in Fig. 3 (b) and (c). The optical lattice is generated by two interfering laser beams (830 nm) crossing under an angle of  $10^\circ$ . The angle is chosen such that the distance between the two wells is larger than the optical resolution of  $3.2(2) \mu\text{m}$  (sparrow-criterion). The barrier is ramped up in 300 ms in order to prevent

excitation of the condensates in each well and to guarantee thermal equilibrium. The coupling strength due to tunneling between the two wells can be adjusted by changing the barrier height. Typically, we vary  $V_0/h$  between 500 Hz and 2500 Hz (the chemical potential ranges between 600 Hz and 900 Hz). Under these conditions, the distance between the two wells is approximately  $4.4 \mu\text{m}$  as shown in Fig. 3 (c).

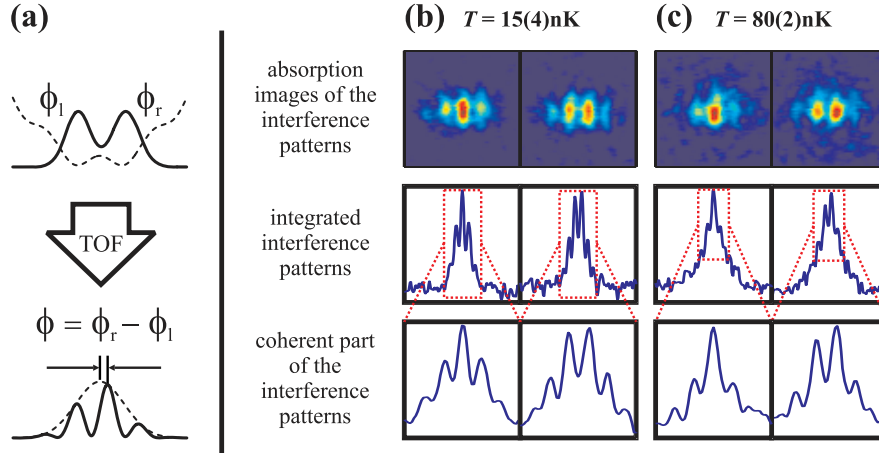


**Figure 4.** Matter-wave interference patterns. (a) is a sketch of the interference experiments. Once the double-well trap is turned off, the matter-wave packets expand, overlap and interfere. (b) corresponds to typical interference patterns for low temperature and (c) to typical interference patterns for high temperature. The integrated patterns show a clear interference signal for all temperatures (central graphs). However, for high temperature also a broad background is visible, corresponding to the distribution of the thermal atoms after the expansion time. In order to find the coherent interference patterns, this background is subtracted (lower graphs).

The relative phase between the two condensates is measured after a time of flight of 5 or 6 ms. Typical interference patterns are shown in Fig.4 (b) and (c). Fig.4 (b) corresponds to measurements at low temperature ( $T = 15(4) \text{ nK}$ ) and (c) to high temperature ( $T = 80(2) \text{ nK}$ ). The single images show a clear interference signal with high visibility (usually larger than 50%). In order to fit the relative phase, the images are integrated transversally to the interference patterns (central graphs). At high temperature a broad incoherent background becomes visible resulting from the ballistic expansion of the thermal atoms. To fit the interference patterns at high temperature, this background is subtracted. The resulting profiles (lower graphs) thus correspond only to the coherent part of the matter wave interference. The fitting procedure leads to an uncertainty of the relative phase of about  $0.13\pi$ .

Repeating the interference experiments reveals that the relative phase is not constant but fluctuates around zero as shown in Fig. 5. The fluctuations increase with increasing temperature and decrease with increasing tunneling coupling. This shows qualitatively that two competing processes are relevant for the thermally induced fluctuations of the relative phase, namely thermal effects leading to a randomization of

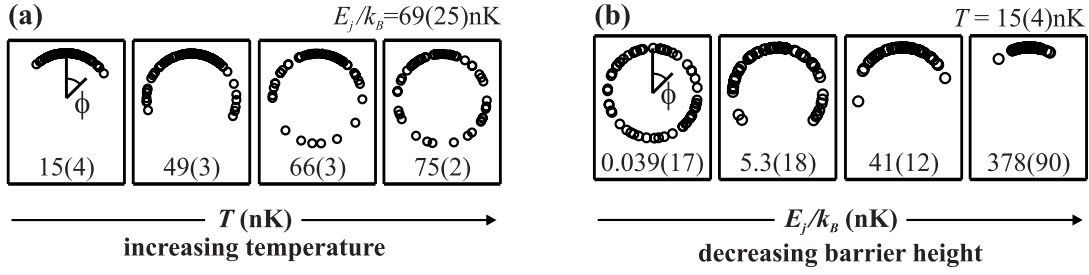


**Figure 5.** Qualitative behavior of the fluctuations of the relative phase. The black circles correspond to single measurements of interference patterns in a polar plot. (a) shows the change of the fluctuations as a function of temperature where the coupling strength is kept constant. With increasing temperature the fluctuations increase. (b) shows the behavior of the fluctuations for decreasing barrier heights leading to an increase of the coupling strength. The temperature is kept constant. Due to the increase of the coupling the fluctuations are decreased demonstrating the stabilizing effect of the tunneling coupling.

the phase and the coherent tunneling coupling to a stabilization of the phase.

#### 4. Coherence factor - scaling law for phase fluctuations

The coherence factor  $\alpha$  (Eq. 19) is a measure for the fluctuations of the relative phase [11] and is directly connected to the visibility of the ensemble averaged interference patterns as discussed in Sec. 2.2. For large  $k_B T/E_J$  the phase fluctuates strongly from shot to shot and causes a reduction of the ensemble averaged visibility. This corresponds to a small coherence factor as visualized in Fig. 6 (a). By increasing the tunneling coupling the coherence of the system can be regained as shown in Fig. 6 (b).

The quantitative measurement of the coherence factor  $\alpha$  as a function of the scaling parameter  $k_B T/E_J$  is shown in Fig. 6 (c). For this, we performed up to 100 measurements with a condensate fraction ranging between 1000 and 4000 atoms at different temperature and different barrier heights (which means that at high temperatures the total number of atoms is approximately 10000). In Fig. 6 (c) every data point corresponds to a subset extracted from these measurements for different atom number ranges (e.g. 2000 to 2500, 2500 to 3000 etc. atoms in the condensate fraction). The Josephson energy  $E_J$  is then calculated for every point at the given trap parameters and the mean atom numbers in the BEC by numerically solving the Gross Pitaevskii equation in 3-D. The influence of the thermal atoms is neglected. Each data point represents at least 28 single measurements and on average 40 measurements. The coherence factor is calculated by averaging over the cosine of the fitted phases.

The temperature corresponding to the data points is measured with three different methods. In the single interference images it is possible to fit the thermal background transversally to the interference patterns. The temperature is then connected to the waist of the thermal cloud and to the time of flight. Additionally, independent time of flight measurements are performed releasing the atoms from the harmonic trap and

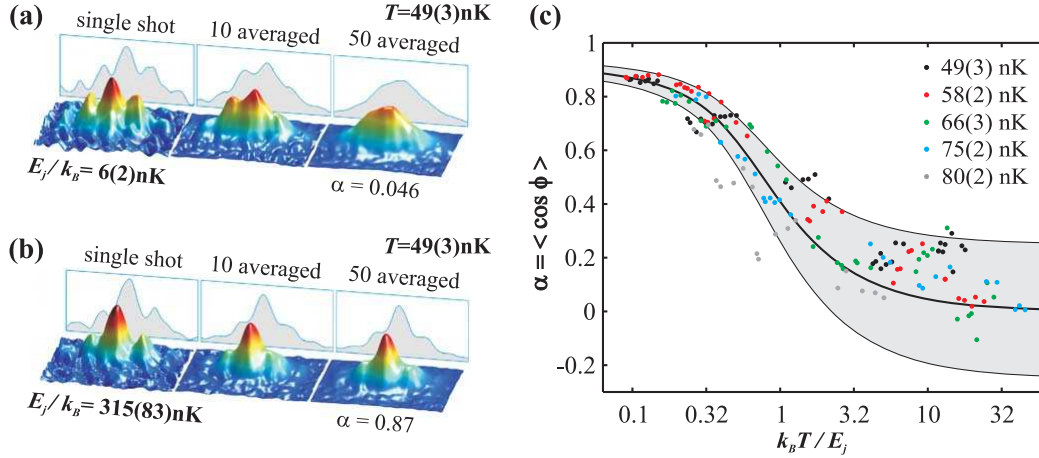


**Figure 6.** Experimental investigation of the coherence factor  $\alpha$ . (a) shows the transition from coherent single realizations to incoherent ensemble averages. The first picture shows that for single realizations a clear interference picture is observed. For small tunneling coupling ( $E_J = 6(2)$  nK) compared to the thermal energy ( $T = 49$  nK) the averaging over many images leads to the loss of the visibility which is directly connected to the loss of the coherence ( $\alpha = 0.046$ ). (b) visualizes that for large coupling ( $E_J = 315(83)$  nK) the averaging over many realizations does not destroy the coherence ( $\alpha = 0.87$ ) and leads only to a small degradation of the visibility. (c) shows the quantitative behavior of the coherence factor  $\alpha$  as a function of the scaling parameter  $k_B T / E_J$ . Each data point corresponds to the averaging over at least 28 (in average 40) single measurements for different  $T$  and  $E_J$ . The temperature is measured independently with time of flight measurements and the coupling strength is deduced from 3-D simulations of the BJJ using independently measured system parameters (potential parameters and atom numbers). The experimental error of  $k_B T / E_J$  is about  $\pm 30\%$ . The central black line corresponds to the prediction of the classical theory and also takes the uncertainty of the phase-fitting into account. The grey shaded area shows twice the expected standard deviation of the coherence factor due to the finite number of measurements. The behavior of the coherence factor is confirmed over a three orders of magnitude change of the scaling parameter.

the temperature deduced from both the expansion velocity of the thermal cloud and the ratio between condensate and thermal fraction. All three methods lead within the experimental error to the same results. The temperatures used for  $k_B T / E_J$  in Fig. 6 (c) are extracted from the time of flight measurements using the last method.

The typical error of  $k_B T / E_J$  is  $\pm 30\%$ . The error in  $E_J$  results from the uncertainty of the atom numbers, the trapping frequencies, the barrier height and the lattice spacing of the periodic potential. The error in  $T$  results from the fitting error of the waists and amplitudes of the double gaussian distribution of the independent time of flight measurements.

The central black line in Fig. 6 (c) shows the theoretical prediction for the coherence factor taking the fitting error of the relative phases into account. The influence of the fitting error on the coherence factor can be estimated by introducing an additional fluctuating phase and averaging over it. The distribution of the additional phase is

approximated by a box function with a standard deviation corresponding to the fitting error. The averaging leads to a reduction of the coherence factor

$$\begin{aligned}
 \alpha' = \langle \cos(\phi) \rangle' &= \frac{\int_{-\phi_0}^{\phi_0} d\phi' \int_{-\pi}^{\pi} d\phi \cos(\phi - \phi') \exp(E_J/k_B T \cos(\phi))}{\int_{-\phi_0}^{\phi_0} d\phi' \int_{-\pi}^{\pi} d\phi \exp(E_J/k_B T \cos(\phi))} \\
 &= \frac{\sin(\phi_0) \int_{-\pi}^{\pi} d\phi \cos(\phi) \exp(E_J/k_B T \cos(\phi))}{\phi_0 \int_{-\pi}^{\pi} d\phi \exp(E_J/k_B T \cos(\phi))} \\
 &= \frac{\sin(\phi_0)}{\phi_0} \cdot \alpha. \tag{20}
 \end{aligned}$$

For our experiments  $\phi_0$  is equal to  $0.23\pi$  which corresponds to a fitting error of  $\sqrt{\frac{1}{2\phi_0} \int_{-\phi_0}^{\phi_0} \phi^2 d\phi} = 0.13\pi$  of the relative phase and to a reduction of the coherence factor  $\alpha' = 0.92\alpha$ . The grey shaded area shows twice the standard deviation of the coherence factor resulting from the finite number of measurements. For about 40 measurements it can be estimated by  $\Delta\alpha \approx (1 - \alpha)/8$ .

The observed behavior of the coherence factor is consistent with the two mode model prediction over three orders of magnitude of the scaling parameter  $k_B T/E_J$ . For small values of  $k_B T/E_J$  the coherence factor is in close agreement with the theoretical prediction. However, for  $k_B T/E_J > 2$  the data points lie within the experimental error but are mainly localized above the curve. This deviation can be explained by the fact that the BJJ is not thermalized for small  $E_J$  (see Sec. 6). The points correspond to high temperature lie outside the shaded region showing a lower degree of coherence. A disagreement in this regime can also be expected as the temperature of 80 nK is close to the critical temperature of  $T_c \approx 87$  nK. In this regime, the excitation spectrum may not be correctly accounted for by the two mode model.

## 5. Thermalization

The theoretical prediction for the coherence factor is only valid in thermal equilibrium. In order to check for thermal equilibration, different experimental tests have been performed.

We have compared the fluctuations of the relative phase after three different ramping schemes as shown in Fig. 7 (a). For these measurements the atom number is 4000(400). In scheme 1, the barrier is ramped up to a low value ( $V_0 = 1140$  Hz) within 300 ms and then kept the barrier constant for 400 ms. Scheme 2 is similar to scheme 1 but with a higher final value of the barrier ( $V_0 = 1450$  Hz). As expected, the fluctuations are small for scheme 1 and larger for scheme 2. Scheme 3 is a combination of the two previous schemes. Initially the barrier is ramped up to the higher value ( $V_0 = 1450$  Hz) within 300 ms, then the barrier is kept constant for 100 ms and then the barrier is ramped down to the lower value ( $V_0 = 1140$  Hz) within 300 ms. The fluctuations measured according to scheme 3 are smaller than those measured according to scheme 2, indicating a thermalization process. This leads to the counterintuitive behavior that phase fluctuations can be decreased by thermalization processes.

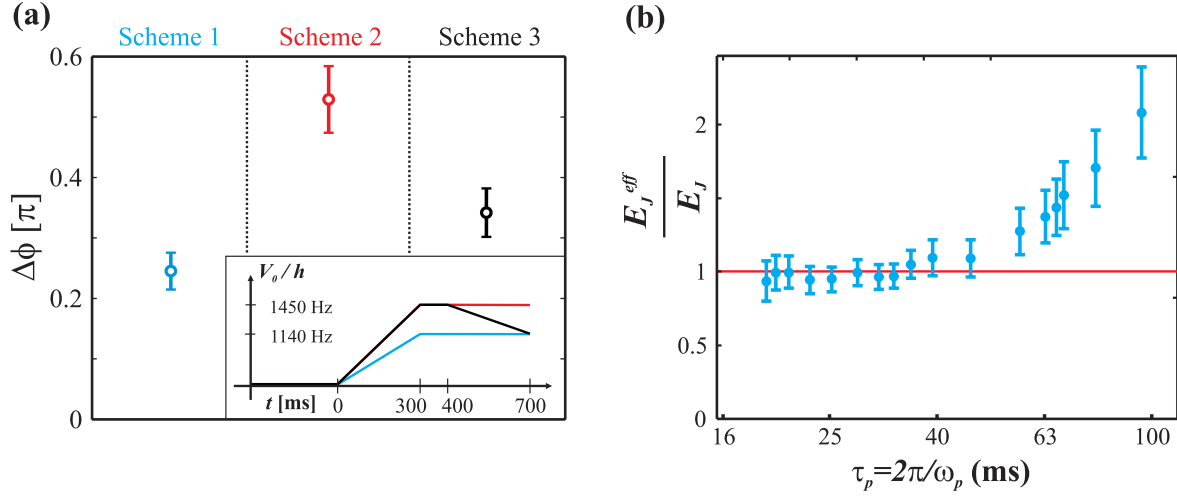


**Figure 7.** Experimental test for thermal equilibration of the BJJ. In (a) three different ramps as indicated are compared. The decrease of the fluctuations for scheme 3 with respect to scheme 2 indicates the thermalization process and the stabilizing effect of the tunneling coupling. (b) shows the comparison of the measured coherence factors and the theoretical expectation. The experimental  $E_J^{\text{eff}}$  are deduced by fitting the measured coherence factor to the theoretical prediction. For tunneling times  $\tau_p \leq 50$  ms the ratio is 1 and no correction is needed. For  $\tau_p > 50$  ms the ratio increases as the BJJ is not completely thermalized. Thermalization takes only place if  $\tau_p \ll t_{\text{ramp}} = 300$  ms, which is the time for ramping up the potential barrier.

To get a more quantitative handle on thermalization we compare the coherence factor measurements with the theoretical prediction from Eq. 19. We introduce an effective tunneling coupling  $E_J^{\text{eff}}$  to account for out of equilibrium situations and deduce  $k_B T/E_J^{\text{eff}}$  from the experimental data shown in Fig. 6. In Fig. 7 (b) the ratio  $E_J^{\text{eff}}/E_J$  is shown as a function of the tunneling time  $\tau_p = 2\pi/\omega_p \propto 1/\sqrt{E_J}$ . We find that for the chosen ramping time of 300 ms the effective tunneling coupling is only equal to the numerically calculated tunneling coupling for  $\tau_p < 50$  ms. Thus for the application as a primary thermometer care has to be taken to choose the appropriate tunneling parameters. The observed increase of  $E_J^{\text{eff}}$  for large tunneling times ( $\tau_p > 50$  ms which corresponds to  $E_J < 60$  nK), could be explained by the fact that the system may still have not reached equilibrium after the 300 ms ramp.

## 6. Application of the thermometer to heat capacity measurement

From the previous discussion it follows that if the tunneling rate is sufficient to guarantee thermal equilibrium ( $\tau_p < 50$  ms for a 300 ms ramping up time of the potential barrier), the measurement of the phase fluctuations and an independent determination of the coupling strength  $E_J$  constitute a primary thermometer.

To test the applicability of the new thermometer we measure the heating up of a degenerate Bose gas in a 3-D harmonic trap. The results are shown in Fig. 8. The blue points correspond to temperature measurements using the phase fluctuation method and

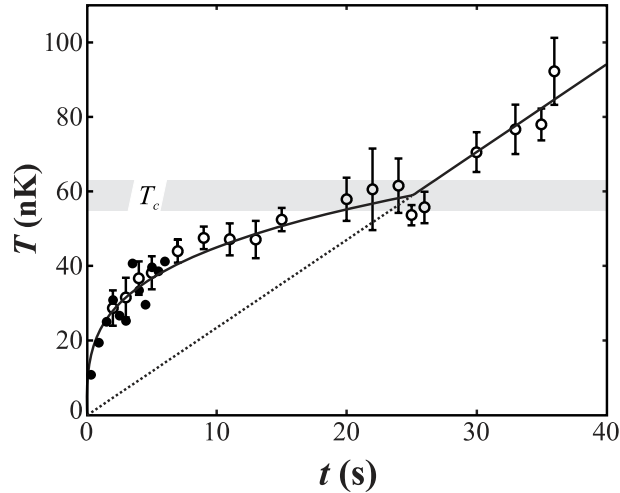


**Figure 8.** Thermometry using phase fluctuations measurements. The graph shows the application of the phase thermometer. The temperature of a degenerate Bose gas is plotted as a function of the holding time in the harmonic trap. The blue points correspond to measurements using the phase fluctuation method (for the few points where  $\tau_p > 50$  ms we slightly correct the calculated temperatures using the effective Josephson energy plotted in Fig. 7 (b)) and the open circles to measurements applying the standard time of flight method. In the overlap region both methods lead to the same results showing the applicability of the noise thermometer. The black line corresponds to a fitting function assuming a constant transfer rate of energy, a power law for the temperature dependent heat capacity below the critical temperature and a constant heat capacity above. The measurements demonstrate the deviation of the heat capacity of the Bose gas from the classical gas.

the open circles to measurements using the standard time of flight method. We observe the heating after a holding time of up to 36 s. After 25 s the critical temperature of  $T_c = 59.1$  nK is reached and the condensate fraction vanishes. For these measurements the total number of atoms in the trap is kept constant, thus the phase fluctuation measurements can only be performed up to 6 s as long as the condensate fraction is large enough to observe clear interference patterns. Below 30 nK the time of flight method cannot be applied as the fraction of thermal atoms in this regime is too small and cannot be fitted.

The increase of the temperature with time can be explained by taking the dependence of the heat capacity on temperature of a Bose gas into account and assuming a constant transfer of energy. For short holding times a fast increase of the temperature corresponding to a large heating rate can be observed. The heating rate decreases continuously until the critical temperature is reached, above the critical temperature the heating rate stays constant. We attribute this decrease of the heating rate to an increase in the specific heat as expected for a degenerate Bose gas. We assume the specific heat to be proportional to  $(T/T_c)^d$  below  $T_c$  and constant afterwards [23]. The

expected evolution of the temperature with time  $t$  is then

$$T(t) = \begin{cases} \sqrt[d+1]{(d+1)h_0T_c^d t + T(0)^{d+1}} & \text{for } T_{\text{fit}} < T_c \\ h_0 t & \text{for } T_{\text{fit}} \geq T_c \end{cases}, \quad (21)$$

where  $h_0$  is the constant energy transfer rate and the critical temperature is deduced from independent measurements of the trap parameters and atom numbers  $T_c \approx 0.94 \cdot \hbar/k_B \cdot (\omega_x \omega_y \omega_z)^{1/3} \cdot N^{1/3} = 59.1$  nK. Using this function to fit the observed temperature increase, we obtain  $h_0 = 2.4(1)$  nK and a dimensionality parameter  $d = 2.4(4)$ . These observations represent the extension to the low temperature limit of the heat capacity measurements already performed in the early days of BEC [24]. The data clearly reveal that the heat capacity of a degenerate interacting Bose gas is smaller than the classical gas prediction for temperatures below  $0.7 \cdot T_c$ . The deduced dimensionality is slightly smaller than the theoretical prediction  $d = 3$  for the heat capacity of an ideal Bose gas confined in a 3-D harmonic trap. This is also expected due to the presence of atom-atom interaction [25]. Clearly the dependence of the heat capacity on the temperature with  $d > 1$  confirms the prediction of the third law of thermodynamics [26] stating that the heat capacity has to vanish in the zero temperature limit.

## 7. Conclusion

In summary we have presented a detailed analysis of a new method for measuring ultralow temperatures of degenerate Bose gases in a regime where standard time of flight methods cannot be applied. These temperature measurements were done by investigating thermally induced fluctuations of the relative phase between two weakly coupled Bose-Einstein condensates. We have compared the experimentally obtained coherence factor with the theoretical prediction using a standard two mode model at finite temperature. We found quantitative agreement over a wide range of the relevant scaling parameter. With this a primary thermometer is realized. The application of this noise thermometer was demonstrated by measuring the heating up of a quantum degenerate Bose gas. The observed temperature increase reveals in a direct way that the heat capacity of the Bose gas below the critical temperature deviates strongly from the heat capacity of a classical gas and vanishes in the zero temperature limit as predicted by the third law of thermodynamics.

## Acknowledgments

We thank T. Bergeman very much for the numerical calculation of the relevant parameters and the valuable theoretical support. We would also like to thank A. Trombettoni for discussions, M. Albiez and J. Foelling for their contributions to the experiments, M. Scherer for implementing the 3D Gross-Pitaevskii code, and D. Weiskat for his indispensable help with the electronics. This work was funded by Deutsche

Forschungsgemeinschaft Schwerpunktsprogramm SPP1116 and by Landesstiftung Baden-Württemberg - Atomoptik. R. G. thanks the Landesgraduiertenförderung Baden-Württemberg for the financial support.

## References

- [1] T Schumm, S Hofferberth, L M Andersson, S Wildermuth, S Groth, I Bar-Joseph, J Schmiedmayer, and P Krueger. Matter-wave interferometry in a double well on an atom chip. *Nat. Phys.*, 1:57–62, 2005.
- [2] M Saba, T A Pasquini, C Sanner, Y Shin, W Ketterle, and D E Pritchard. Light scattering to determine the relative phase of two Bose-Einstein condensates. *Science*, 307:1945, 2005.
- [3] M Albiez, R Gati, J Foelling, S Hunsmann, M Cristiani, and M K Oberthaler. Direct observation of tunneling and nonlinear self-trapping in a single bosonic josephson junction. *Phys. Rev. Lett.*, 95:010402, 2005.
- [4] K K Likharev. Superconducting weak links. *Rev. Mod. Phys.*, 51:101–169, 1979.
- [5] A Barone and G Paterno. *Physics and applications of the Josephson effect*. Wiley, New York, 1982.
- [6] J C Davis and R E Packard. Superfluid  $^3\text{He}$  Josephson weak links. *Rev. Mod. Phys.*, 74:741–773, 2002.
- [7] F Sols. Randomization of the phase after suppression of the Josephson coupling. *Physica B*, 194-196:1389–1390, 1994.
- [8] A Imamoglu, M Lewenstein, and L You. Inhibition of coherence in trapped Bose-Einstein condensates. *Phys. Rev. Lett.*, 78:2511–2514, 1997.
- [9] A J Leggett. Bose-Einstein condensation in the alkali gases: Some fundamental concepts. *Rev. Mod. Phys.*, 73:307–356, 2001.
- [10] L Pitaevskii and S Stringari. Thermal vs quantum decoherence in double well trapped Bose-Einstein condensates. *Phys. Rev. Lett.*, 87:180402, 2001.
- [11] R Gati, B Hemmerling, J Foelling, M Albiez, and M K Oberthaler. Noise thermometry with two weakly coupled Bose-Einstein condensates. *Phys. Rev. Lett.*, 96:130404, 2006.
- [12] M R Andrews, C G Townsend, H-J Miesner, D S Durfee, D M Kurn, and W Ketterle. Observation of interference between two Bose condensates. *Science*, 275:637–641, 1997.
- [13] S Dettmer, D Hellweg, P Ryytty, J J Arlt, W Ertmer, K Sengstock, D S Petrov, G V Shlyapnikov, H Kreutzmann, L Santos, and M Lewenstein. Observation of phase fluctuations in elongated Bose-Einstein condensates. *Phys. Rev. Lett.*, 87:160406, 2001.
- [14] S Richard, F Gerbier, J H Thywissen, M Hugbart, P Bouyer, and A Aspect. Momentum spectroscopy of 1D phase fluctuations in Bose-Einstein condensates. *Physical Review Letters*, 91(1):010405, 2003.
- [15] D Ananikian and T Bergeman. Gross-pitaevskii equation for Bose particles in a double-well potential: Two-mode models and beyond. *Phys. Rev. A*, 73:013604, 2006.
- [16] G J Milburn, J Corney, E M Wright, and D F Walls. Quantum dynamics of an atomic Bose-Einstein condensate in a double well potential. *Phys. Rev. A*, 55:4318–4324, 1997.
- [17] J R Anglin and A Vardi. Dynamics of a two-mode Bose-Einstein condensate beyond mean-field theory. *Phys. Rev. A*, 64(1):013605, May 2001.
- [18] J A Dunningham and K Burnett. Sub-shot-noise-limited measurements with Bose-Einstein condensates. *Physical Review A (Atomic, Molecular, and Optical Physics)*, 70(3):033601, 2004.
- [19] R W Spekkens and J E Sipe. Spatial fragmentation of a Bose-Einstein condensate in a double-well potential. *Phys. Rev. A*, 59:3868–3877, 1999.
- [20] G-S Paraoanu, S Kohler, F Sols, and A J Leggett. The Josephson plasmon as a Bogoliubov quasiparticle. *At. Mol. Opt. Phys.*, 34:4689–4696, 2001.
- [21] S Raghavan, A Smerzi, S Fantoni, and S R Shenoy. Coherent oscillations between two weakly

- coupled Bose-Einstein condensates: Josephson effects,  $\pi$  oscillations, and macroscopic quantum self-trapping. *Phys. Rev. A*, 59:620–633, 1999.
- [22] R Gati, M Albiez, J Foelling, B Hemmerling, and M K Oberthaler. Realization of a single Josephson junction for Bose-Einstein condensates. *Appl. Phys. B*, 82:207–210, 2006.
- [23] S R De Groot, G J Hooyman, and C A ten Seldam. On the Bose-Einstein condensation. *Proc. Roy. Soc. Lond. A*, 203:266–286, 1950.
- [24] J R Ensher, D S Jin, M R Matthews, C E Wieman, and E A Cornell. Bose-Einstein condensation in a dilute gas: Measurement of energy and ground-state occupation. *Physical Review Letters*, 77(25):4984–4987, 1996.
- [25] A Minguzzi, S Conti, and M P Tosi. The internal energy and condensate fraction of a trapped interacting Bose gas. *Journal of Physics: Condensed Matter*, 9(5):L33–L38, 1997.
- [26] R P Feynman, R B Leighton, and M Sands. *The Feynman Lectures on Physics Vol. 1*. Addison-Wesley, Reading, MA, 1963.